Global climate disruption and regional climate shelters after the Toba supereruption

Benjamin A. Black[1,2,3], Jean-François Lamarque[4], Daniel R. Marsh[4,5], Anja Schmidt[6,7], Charles Bardeen[8]

[1]Earth and Atmospheric Science, City College of New York, New York, NY 10031. [2]Earth and Environmental Sciences, Graduate Center, City University of New York, New York, NY 10017. [3]Department of Earth and Planetary Sciences, Rutgers University, New Brunswick, NJ (bblack@eps.rutgers.edu) [4]Climate and Global Dynamics Lab, National Center for Atmospheric Research, Boulder, CO. [5]Faculty of Engineering and Physical Sciences, University of Leeds, Leeds, UK [6]Department of Chemistry, University of Cambridge, Cambridge, UK. [7]Department of Geography, University of Cambridge, Cambridge, UK. [8]Atmospheric Chemistry Observations and Modeling Lab, National Center for Atmospheric Research, Boulder, CO.

Abstract

The Toba eruption ~74,000 years ago was the largest volcanic eruption since the start of the Pleistocene, and represents an important test case for understanding the effects of large explosive eruptions on climate and ecosystems. However, the magnitude and repercussions of climatic changes driven by the eruption are strongly debated. High-resolution paleoclimate and archaeological records from Africa find little evidence for disruption of climate or human activity in the wake of the eruption, in contrast with a controversial link with a bottleneck in human evolution and climate model simulations predicting strong volcanic cooling for up to a decade after a Toba-scale eruption. Here we use a large ensemble of high-resolution Community Earth System Model (CESM1.3) simulations to reconcile climate model predictions with paleoclimate records, accounting for uncertainties in the magnitude of Toba sulfur emission with high and low emission scenarios. We find a near-zero probability of annual-mean surface temperature anomalies exceeding 4 °C in most of Africa, in contrast with near 100% probabilities of cooling this severe in Asia and North America for the high sulfur emission case. The likelihood of strong decreases in precipitation is low in most of Africa. Therefore, even Toba sulfur release at the upper range of plausible estimates remains consistent with the muted response in Africa indicated by paleoclimate proxies. Our results provide a probabilistic view of the uneven patterns of volcanic climate disruption during a crucial interval in human evolution, with implications for understanding the range of environmental impacts from past and future super-eruptions.

Significance statement

The Younger Toba Tuff is the largest volcanic eruption of the past 2 million years, but its climatic consequences have been strongly debated. Resolving this debate is important for understanding environmental changes during a key interval in human evolution. This work uses a large ensemble of global climate model simulations to demonstrate that the climate response to Toba was likely to be pronounced in Europe, North America, and central Asia and muted in the Southern Hemisphere. Our results reconcile the simulated distribution of climate impacts from the eruption with paleoclimate and archaeological records. This probabilistic view of climate disruption from Earth's most recent supereruption underscores the uneven expected distribution of societal and environmental impacts from future very large explosive eruptions.

Main text

The eruption of the Younger Toba Tuff from Toba caldera in Sumatra, Indonesia, expelled a ~2,800 km^3 dense-rock equivalent volume of magma, generating an eruption column and co-ignimbrite cloud that reached an altitude of 30-40 km (1, 2). As the largest eruption of the past 2 million years, the Toba eruption represents an important benchmark for understanding the climate consequences of supereruption-scale volcanism. However, the environmental effects of the 73.88 ± 0.32 ka Toba eruption are strongly contested, especially in Africa (3-7). The eruption occurred during a critical juncture in hominin evolution, when early humans were poised to expand more broadly beyond Africa (8). Ash from the eruption was transported thousands of kilometers, forming a widely used chronologic marker for stratigraphic sections across Africa and Asia (9, 10). The recent identification of Toba cryptotephra in two archaeological sites in southern Africa demonstrates that early humans in these locations flourished through the eruption interval (11). These records contrast with the controversial proposal that a severe volcanic winter (12-14) decimated early humans (15). Tephrochronologically calibrated records from Lake Malawi in Eastern Africa also reveal a striking lack of cooling or ecological disruption directly following the eruption (4, 7), underscoring the discrepancy between some model-based expectations and recorded climate effects from Toba.

Sulfate aerosols from large explosive eruptions are known to cause a net decrease in downwelling shortwave radiative flux, with repercussions for Earth's surface temperatures, ocean circulation, hydrology, and the large-scale circulation of the atmosphere (16-18). However, aerosol-climate models suggest that there is a non-linear relationship between the severity of these effects and increasing eruption size, with more rapid aerosol settling and less efficient radiative interactions as aerosol sizes increase with successively larger SO_2 emissions from explosive eruptions (19, 20). Estimated sulfur emissions from the Toba eruption span two orders of magnitude, ranging from 70−6,600 Tg of SO_2, equivalent to approximately 10-360× the sulfur emissions from the 1991 eruption of Mt. Pinatubo (21, 22). Previous climate model simulations of the Toba eruption have included single idealized simulations (23) and individual aerosol simulations used to force a small climate ensemble with five ensemble members (3, 24). Timmreck et al. (3) found a peak aerosol optical depth of ~14 around one year after the eruption, and a maximum global-mean cooling of ~3.5 °C, with a maximum summertime cooling of ~12 °C over northern hemisphere continental interiors. For comparison, the estimated maximum global- annual-mean cooling after the 1991 eruption of Mt. Pinatubo was ~0.5 °C (25).

Effects of Toba on regional climate in Africa are of particular interest because of the potential implications for human populations there. Climatic variability in eastern and southern Africa is dominated by changes in effective moisture and precipitation driven by seasonal shifts in the intertropical convergence zone (ITCZ; (26, 27)). Rainfall in most of eastern Africa is concentrated into the boreal spring “long rains” and boreal autumn “short rains” of the east African monsoon (28). Just as warming due to increased greenhouse gas emissions can intensify the global hydrological cycle (29), surface cooling due to volcanic sulfate aerosols can temporarily spin down the hydrological cycle, leading to a reduction in global-mean precipitation (17, 18), with significant regional variability that is broadly inverted from the climate response expected under future warming (30). Prior modeling of the climate response to the Toba eruption identified a strong global precipitation anomaly, with the potential for disruption of the Indian monsoon for the first two years after the eruption in addition to decreases in precipitation and primary productivity in Africa (3, 24). Tropical eruptions may also weaken the West African monsoon, one of several proposed mechanisms linking explosive volcanic eruptions with El Niño-like events (31-34).

Significant uncertainties in the climate effects of prehistoric volcanic eruptions arise from the magnitude of sulfur emissions, eruption time of year, background climate state, and sulfur injection altitude. Background climate state is known to strongly influence the climate effects of volcanic aerosols, including hemispheric bias in dispersion of the aerosol cloud driven by shifts in stratospheric circulation (24, 35, 36). Likewise, increasing masses of sulfur emission display a broad—though non-linear and complex—correlation with increased cooling (37, 38). The effects of emissions altitude include impacts on aerosol residence time (35, 37, 39). In this study we employ a large ensemble comprising 42 simulations in which we consider a range in each of these parameters (Table S1), including initialization from different climate background states (at least 5 per sulfur emission scenario) branched from our control run, which does not include the volcanic emissions. We also considered four different times of year for the eruption (Table S1), to account for seasonal changes in stratospheric circulation and aerosol dispersion. By bracketing a plausible range of possibilities for these key parameters, this approach enables us to make a probabilistic assessment of the range of climatic disruptions from Toba. We use the Community Earth System Model version 1.3 (CESM1.3), a three-dimensional (3-D) global climate model that couples atmosphere, ocean, and sea-ice components (40). The atmospheric component of CESM1.3 is the Whole Atmosphere Community Climate Model version 4 (WACCM) (41), which we employ to simulate the physical and chemical impacts of the Toba eruption. WACCM is a chemistry−climate model, with its top boundary located near 140-km geometric altitude. It has a horizontal resolution of 1.9° × 2.5° (latitude × longitude), and variable vertical resolution of 1.25 km from the boundary layer to near 1 hPa, 2.5 km in the mesosphere, and 3.5 km in the lower thermosphere, above about 0.01 hPa. We use the Community Aerosol and Radiation Model for Atmospheres (CARMA), a detailed sectional aerosol microphysics model (42-44) within the CESM framework (see Methods), to investigate both the global climate response to the Toba supereruption and the regional climate response in southern and eastern Africa. This same model version was recently used to simulate the climate impacts associated with soot release following the Chicxulub impact (44). In particular, this model represents the oxidation of volcanic SO_2 and the nucleation, coagulation, growth, and removal of sulfate aerosols (43).

Each simulation was run for 10 years, sufficiently long to capture the peak climate impact in the atmosphere and upper ocean and the overall recovery (45). We consider sulfur emissions of 200 and 2000 Tg SO_2 (see Methods for discussion). For comparison, previous Toba aerosol simulations by Timmreck et al. (3, 24) and English et al. (23) assumed 1700 Tg SO_2 and 2000 Tg SO_2 respectively. Uncertainties in the timing of the Toba eruption relative to the Marine Isotope Stage 4/5 boundary translate to uncertainties in the stadial or interstadial background climate state prior to the eruption (24, 46). We consider boundary conditions appropriate for an interstadial climate state in our simulations, neglecting possible differences in patterns of vegetation cover related to stadial versus interstadial boundary conditions (24). Records of charcoal and plant fossils in cores from Lake Malawi do not show large variations in vegetation across the Toba interval (7). Within each ensemble, simulations were initialized from different states of a 108-year control run, spaced two years apart to ensure we capture different phases of the El Niño Southern Oscillation (ENSO). This large ensemble approach permits us to account for some of the uncertainties related to background climate state including the phase of ENSO (36).

2. Evolution of the Toba sulfate aerosol cloud

Our simulations show strong (>1-2 ˚C) global-mean surface temperature changes lasting a half-decade or more in response to a Toba eruption emitting 200-2000 Tg SO_2, with significant regional variability in the simulated changes (see the following section). Global-mean surface temperatures do not fully recover within the 10-year span of the 2000 Tg SO_2 simulations. In the ocean, the residual thermal effects of large-scale volcanic eruptions have also been shown to extend to multi-decadal timescales (47). In all simulations, the Toba eruption leads to peak aerosol optical depths and maximum surface cooling 6-30 months after the eruption (Fig. 1). Aerosol optical depth (AOD) reaches maximum monthly zonal mean values of 1-2 or 8-10 for 200 or 2000 Tg SO_2 emissions respectively (Figures S1-S3). The global monthly mean AOD reaches a maximum value of ~1.5-2 from 1-2 years after a 2000 Tg SO_2 release, and ~0.4-0.7 after a 200 Tg SO_2 release (Fig. 1, Figs. S1 and S2). Optical depth peaks earlier and aerosol sizes are slightly smaller at 100 hPa for the lower (18-25 km) sulfur injection altitude (Figs. 1, S3, S4), and the residence time of the aerosol cloud in this ensemble is shorter, consistent with previous work (39), but the hemispheric transport of the aerosol cloud is not strongly impacted by injection altitude (Figs. S2, S3; (35, 37)).

Extratropical eruptions generate larger aerosol loading in the hemisphere of eruption. For tropical eruptions such as Toba, seasonal shifts in the large-scale Brewer-Dobson circulation in the stratosphere further modulate the distribution of volcanic aerosols (37, 48). Consequently, eruption seasonality can strongly influence forcing and climate response (36). Hemispherically asymmetric forcing has been linked with migration of the ITCZ away from the hemisphere with stronger volcanic forcing (49, 50) and with divergent consequences for the El Nino Southern Oscillation (51). In line with results from Toohey et al. (48), our simulations with September and December eruptions show higher AOD in the northern hemisphere (Figs. S1,S3). AOD after the June eruption ensemble is roughly hemispherically symmetric, while AOD following a March eruption is stronger in the southern hemisphere (SH), though the March ensemble in particular shows some spread among ensemble members (Fig. S3).

Maximum global-mean cooling is 2.3±0.4 ˚C (1 s.d.) for 200 Tg SO_2 release, and 4.1±0.3 ˚C (1 s.d.) for 2000 Tg SO_2 release (Figure 1), emphasizing the non-linearity of the radiative effects of larger SO_2 release magnitude (3, 19). Maximum global-mean cooling is somewhat sensitive to the time of year of the eruption; maximum cooling for a September eruption is ~1 ˚C larger than for a March eruption (Fig. 1, Fig. S3). For all ensembles, maximum global mean cooling is significant at the 2-sigma level (Fig. 1). Cooling is much more protracted after 2000 Tg SO_2 release, with global-mean surface temperature anomalies exceeding 2 ˚C spanning up to five years after the eruption.

Global-mean surface temperatures recover more slowly than AOD, in particular for the 2000 Tg SO_2 scenario, pointing to slow recovery of ocean heat content (47, 52). Global mean cooling of ~1˚C persists after 10 years in the 2000 Tg SO_2 cases.

For the 200 Tg SO_2 eruption scenarios, global-mean precipitation remains largely within the range of natural variation (Fig. 2). For the 2000 Tg SO_2 eruption scenario, however, precipitation shows a strong decline, with global mean precipitation that is significantly (at the 2-sigma level) outside the range of natural variation lasting ~5 years following the eruption (Fig. 2). This is consistent with slowing of the hydrological cycle associated with a global cooling (53).

3. Regional temperature response patterns and the role of the ocean in modulating the climate response

We next consider the regional climate response to a Toba-scale eruption, focusing particular attention on Africa and India, where paleoclimate proxy and archaeological records synchronized with Toba cryptotephra have been used to evaluate the consequences of the eruption for climate and human populations (6-8, 10, 54). Our simulations show that in the aftermath of a Toba-scale eruption, the regional climate response in southern and eastern Africa is weaker than the global-mean response in terms of both surface temperature and precipitation (Figures 3 and 4). Ultimately, this finding implies that the full range of Toba emissions investigated here (from 200 Tg SO_2 to 2000 Tg SO_2) can be reconciled with the muted climate response observed in proxy records from Africa and possibly India.

For the 200 Tg SO_2 simulations, NH temperature anomalies reach 4-5 °C (Fig. S5), and regional temperature changes in the second year after the eruption are significant with >90% confidence with the exception of some areas in Africa, Antarctica, and South America in the high altitude emissions scenario (Figure S5). As expected, the most severe global and regional temperature impacts occur for emissions of 2000 Tg SO_2. In that case, we find widespread Northern Hemisphere (NH) cooling, regionally exceeding 8-10 °C (Fig. 3) in interior North America and Eurasia, consistent with the strong summertime cooling in these regions found in prior simulations (20, 24). These changes are significant with >90% confidence with the exception of some areas in Antarctica and Africa (Fig. 3A). The likelihood of annual-mean cooling greater than 4 °C in NH continental interiors approaches 100% for the 2000 Tg SO_2 simulations (Figure 5).

For both sulfur emissions levels, we find a more muted surface cooling in response to Toba in the Southern Hemisphere. Even in the March eruption scenario (Fig. S6) in which distribution of the Toba aerosol cloud is primarily in the SH, the climate signal in the SH is relatively weak. The likelihood of annual-mean SH cooling greater than 4 °C is near-zero for both levels of sulfur release (Figure 5). In the absence of an established critical threshold for ecosystem damage from transient cooling, the 4 °C threshold was selected because it approximates the maximum cooling in Africa inferred in previous Toba modeling studies (20, 24) and therefore represents a common point of comparison for previous paleoclimate proxy studies (6, 7). For context, 4 °C cooling is ~4× the magnitude of global warming from 1880-2012 (IPCC AR5). The muted cooling in the Southern Hemisphere, which is consistent with prior work (32, 44, 55, 56), highlights the role of the ocean in modulating the cooling (45, 57) from the stratospheric volcanic aerosol cloud. In addition, the fact that the aerosol cloud is located over the Northern Hemisphere in the majority of our simulations (Figs. S1-S3) leads to a more strongly asymmetric response relative to, for example, CO_2 forcing. This is similar to the asymmetry in the distribution of present-day anthropogenic tropospheric aerosols, which are mostly concentrated in the Northern Hemisphere, and for which the climate response is also concentrated in the Northern Hemisphere (58).

In terms of zonal-mean annual-mean land surface temperature response, we find that the largest impact in the Southern Hemisphere is approximately three times weaker than in the Northern Hemisphere. This result holds true over the full range of SO_2 emission magnitudes (200-2000 Tg SO_2), indicating that this is likely a robust feature of these simulations. Importantly, because the background climate in Africa is relatively temperate, below-freezing temperatures are also much less frequent in Africa than in North America or Asia (Fig. S7), even for the 2000 Tg SO_2 scenario.

Precipitation is another important factor in climate stability, with implications for human activity and ecology (59). Parts of southern Africa and India show marked regional decreases in precipitation in the case of the largest sulfur emission (Figs. 4, S8). While the patterns of precipitation change do reflect a slight ITCZ shift away from the hemisphere with more aerosol (49, 50), in most simulations there is significant aerosol in both hemispheres, and the resulting pattern of ITCZ disruption is complex (Fig. S8). Cooling of the surface ocean, which buffers temperatures on land but leads to a reduction in evaporation (52), provides a potential explanation for the broadly complementary patterns of precipitation and temperature change. The distribution of precipitation changes is consistent with results from Timmreck et al. (24), who found significant decreases in precipitation in the Ganges/Brahmaputra catchment in the first several years after an eruption, followed by increases in years 4 to 5 after an eruption. Impacts on precipitation are less pronounced (Fig. 2, Fig. 5) for the 200 Tg SO_2 simulation ensembles.

In summary, we identify significant regional and hemispheric differences in response to a Toba-scale eruption. The temperature response in Southern Africa is notably smaller in amplitude than the global-mean response, especially in the 0-30 °S latitudinal band. In conjunction with the relatively warm background climate of Africa, this muted cooling only rarely causes temperatures below freezing (Fig. S7). In addition to identifying this mild surface temperature response in Africa—even under the most extreme emissions scenario—we also identify regions showing a more severe surface temperature response, in particular in NH continental interiors. We therefore expand the discussion in the next section to consider the potential implications for hominin populations, using the full range of experiments.

4. Comparison with records of paleoclimate and human activity

The effects of the Toba eruption on both climate and hominin populations has been strongly debated for decades (4, 5, 9, 11). Toba tephra and cryptotephra enable the eruption interval to be pinpointed within paleoclimate and archeological records, permitting temporally precise model-proxy comparisons of the climate and cultural response to the eruption.

At the time of the Toba eruption 74 ka, southern and eastern Africa hosted significant population centers for anatomically modern humans. Substantial controversy surrounds the timing of human dispersal from Africa and thus which hominin populations were present in India and other regions at the time of the Toba eruption (8, 54, 60, 61). In southeast Asia, Middle Paleolithic cultures may have been well established in the Jurreru and Middle Son River valleys (8, 54). Neanderthal populations in Europe were on the eve of a decline that culminated around 40 ka, broadly coinciding with the expansion of anatomically modern humans (62). The emerging archaeological consensus points to striking continuity in hominin activity across the eruption interval in southern Africa and India (8, 11, 54), contrary to early proposals of a volcanic winter that caused a bottleneck in human evolution (15).

One possible interpretation of the archaeological consensus is that of hominin resilience in the face of changing environmental conditions (8). An alternative interpretation is that the environmental disruption due to Toba was modest. This interpretation finds support from paleoclimate records from Lake Malawi, which do not reveal any dramatic changes in the thermal structure of the lake across the Toba interval even at sub-annual resolution (4). This apparently stable climate through the eruption interval is at odds, however, with a cooling of ~4 °C or more predicted from previous climate modeling studies (3, 14, 24).

Our simulations point to a third possibility: that Toba may have had strong effects on surface temperatures, but not in the regions where anatomically modern humans were thriving. We find that there is a <5% likelihood of annual-mean surface cooling exceeding 4 °C across virtually all of sub-Saharan Africa and India, even in response to 2000-Tg SO_2 emissions (Figure 5). This level of SO_2 emissions is an upper bound on the estimated sulfur release from Toba (21, 22), and the chance of >4 °C cooling after a 200 Tg SO_2 injection is even smaller. Because the muted climate response in Africa—consistent with paleoclimate evidence—is a feature of both our 200 Tg SO_2 and 2000 Tg SO_2 simulations, our results do not allow us to independently exclude either emissions scenario. In contrast with the modest changes in surface temperature in Africa, both levels of sulfur emission are likely to cause strong cooling in Europe and Asia (Figs. 5 and S5).

Our simulations thus suggest that Africa and India could have served as shelters from transient cooling in the aftermath of Toba. As discussed above, in the 2000 Tg SO_2 Toba scenario, strong reductions in precipitation are possible in India, with less pronounced changes in precipitation in the 200 Tg SO_2 Toba scenario. If the Toba eruption did indeed release 2000 Tg SO_2 rather than lower estimates—which remains uncertain—it implies that the hominin populations inhabiting India continuously across the eruption interval exhibited substantial resilience in the face of transient disruption to precipitation patterns.

For all of our Toba scenarios, climate conditions in Europe and most of Asia are predicted to be severe following the eruption. For the highest sulfur emissions we considered, our simulations indicate annual-mean cooling of up to 10 °C in Europe and Asia. Europe was home to significant populations of Neanderthals at this time, while the related Denisovan lineage occupied southern Siberia (Figures 3A and 4A; (60, 63)). Although the available archaeological evidence is insufficient to evaluate effects on hominin populations in those regions, the effects of Toba on these populations thus merit future investigation, in particular if Toba cryptotephra can be identified.

5. Probabilistic climate effects of very large explosive eruptions

In addition to the specific application to the Toba eruption ~74,000 years ago, our large ensemble results also offer more general insights into large explosive tropical eruptions. The range of sulfur emissions we consider, from 200 to 2000 Tg SO_2, would be representative of a sulfur-rich explosive eruption with a Volcanic Explosivity Index of 7 to 8. The 1257 Samalas eruption injected an estimated 126-150 Tg SO_2 into the stratosphere (64), whereas the Tambora eruption of 1815 released ~50-60 Tg SO_2 (57). The 21.8 Ma Fish Canyon Tuff, the largest known silicic eruption, may have released ~10^4 Tg SO_2 (21).

Uncertainties and gaps in records of sulfur emissions for older eruptions challenge precise determination of the frequency distribution of large-magnitude stratospheric sulfur injections. However, the presence of at least two Plinian eruptions in the past millennium with SO_2 release >100 Tg SO_2—Kuwae in 1453 and Samalas in 1257—suggests that explosive eruptions with sulfur emissions within a factor of two of the lower end of our simulated emissions range are likely to recur on millennial timescales. Because of the complex effects of volcanic eruptions on the climate system, no shelter is likely to be completely isolated from volcanically induced climate signals. However, our simulations, in conjunction with other modeling studies (32, 57), indicate that southern Africa and India are relatively insulated from the cooling caused by equatorial or northern hemisphere large explosive volcanic eruptions, and therefore may have been partial shelters from climatic stress related to prehistoric explosive volcanism.

We address the uncertainty in the background state of the stratospheric circulation (66) by considering an ensemble spanning summer, fall, winter, and spring. We note that the availability of paleorecords of eruption time of year would improve constraints on the expected climate response. The Lake Challa record, which promises even higher temporal resolution than the Lake Malawi record (4, 67), may enable determination of the season of the Toba eruption.

In summary, our results indicate that regional changes in climate in response to the Toba eruption have complex distributions and depart markedly from the magnitude of global-mean signals. Large ensembles of climate simulations provide a valuable tool to obtain probabilistic estimates of the distribution of expected climate impacts of eruptions. Understanding regional climate response is necessary to relate volcanic perturbations to proxies for local- to regional-scale climate, to understand temporal changes in climate relevant to hominin evolution and migration, and to inform estimates of the climate effects of large-scale sulfur release from future explosive eruptions.

Methods

CESM 1.3 is a global climate model that includes detailed sub-models of the Earth's atmosphere, oceans, land, and sea ice to comprehensively simulate coupled Earth systems (40). For this work we include the high-top version of the atmosphere model, the Whole Atmosphere Community Climate Model (WACCM; (68)), which extends through 66 vertical levels to an altitude of approximately 140 km. To track the evolution of the Toba aerosol cloud, we include the Community Aerosol and Radiation Model for Atmospheres (CARMA), a three-dimensional sectional (binned) aerosol microphysical model (42-44) that includes 30 aerosol size bins. WACCM/CARMA includes reactions among sulfur-bearing species as tabulated in (43) with reaction rates from (69). The model tracks oxidation of S-bearing gases (in this case SO_2) and nucleation to form sulfate aerosols; condensational growth and coagulation; deposition and sedimentation (see (37) for more detailed discussion of the model). Tracking these processes is critical to accurately computing the radiative effects of very large eruptions because of self-limiting microphysical and chemical processes (19). We completed 22 simulations with 2000 Tg SO_2 emissions and 20 simulations with 200 Tg SO_2 emissions in which we varied sulfur release altitude, time of year of eruption, and background climate through initialization from different states of the control run (see Table S1).

Volcanic forcing. The sulfur release from the Younger Toba Tuff (YTT) eruption is uncertain. Constraints from petrology and ice core records each incorporate significant unknowns (22). The YTT has been correlated with one of the largest sulfur peaks in the GISP2 ice core, representing sulfur loading of 1100-2200 Tg SO_2 (70); however this correlation is somewhat circular in that the attribution of the sulfate peak in the ice core is primarily based on the expectation of strong YTT sulfur loading. More recent work has identified several bipolar sulfate peaks in Greenland and Antarctic ice core records in the interval 74.1–74.5 ka that are candidates to represent the YTT eruption (46, 71). Petrologically, sulfur concentrations in the rhyolitic Toba magma are likely to be lower than in more mafic magmatic systems like that of Mount Pinatubo (22). Indeed, sulfur concentrations in YTT melt inclusions overlap with sulfur in matrix glasses (72). Owing to the tendency of sulfur to partition into a coexisting fluid phase (73, 74), the sulfur yield depends strongly on the extent of excess sulfur. Sulfur partitioning into a fluid phase depends on oxygen fugacity (21). Scaillet et al. (21) argued that the YTT magma chamber likely lacked an exsolved S-rich fluid, and therefore suggested limited sulfur degassing of only ~70 Tg SO_2. However, estimates of oxygen fugacity in the quartz-bearing YTT magmas relative to the Ni-NiO buffer range from approximately ΔNNO=-0.5 to +1.1 (75, 76). This corresponds to an order of magnitude variation in sulfur partitioning between fluid and melt (21), implying sulfur from coexisting fluid could potentially have been more important than recognized by (21).

Given uncertainties in YTT sulfur yields, and to explore the sensitivity of our results to sulfur emissions, we therefore considered high and moderate sulfur injection scenarios in our simulations. For consistency with the study of (23), we selected 2000 Tg SO_2 as our high sulfur injection scenario and 200 Tg SO_2 as our more conservative sulfur injection scenario. For comparison, these emissions scenarios respectively represent

~100× and ~10× the estimated stratospheric sulfur injection of the 1991 eruption of Mount Pinatubo in the Philippines. The 1257 Samalas eruption in Indonesia released 158±12 Tg SO_2 (64), similar to the lower emissions scenario. Recent ice core-based estimates for several candidate YTT layers range from ~150-350 Tg SO_2, bracketing this lower emissions scenario (71). We recognize that the 2000 Tg SO_2 scenario may well exceed the actual sulfur release from the YTT eruption. This is by design, and yields the advantage that because this scenario represents the most extreme case, it enables us to evaluate the potential for sheltered regional climates even assuming a very severe global volcanic event.

Estimates of the YTT eruption column height range from 30-42 km (77). Based on ash dispersal modeling with modern windfields, Costa et al. (77) inferred a best-fit altitude of 42 km, and a best-fit duration of 15 hours. This high plume altitude is consistent with recently reported mass-independent fractionation of sulfur in several candidate YTT layers (71). In most simulations, we therefore distributed SO_2 emissions between 35 and 40 km in the model, spanning 1.9 °S to 13.3 °N and 93.8 °E to 116.2 °E, centered above the Toba caldera. Because sulfur emissions may be distributed over a range in altitude, and to test sensitivity to altitude, we included an ensemble of ten 200 Tg SO_2 simulations at 18-25 km altitude (Table S1).

Statistical significance. To test the statistical significance of surface temperature and precipitation anomalies, we use a Wilcoxon ranked sum test, implemented as the rankedsum function in MATLAB. For each grid cell, we compare the distribution of monthly temperature and precipitation anomalies in Toba simulations with the distribution of monthly temperature and precipitation anomalies relative to a monthly climatology based on our 20-year control run. We specify a p-value of 0.1 for rejection of the null hypothesis that these distributions cannot be distinguished from each other.

Acknowledgments
We acknowledge high-performance computing support from Cheyenne (doi:10.5065/D6RX99HX) provided by NCAR's Computational and Information Systems Laboratory. The CESM project is supported primarily by the National Science Foundation (NSF). This material is based upon work supported by the National Center for Atmospheric Research (NCAR), which is a major facility sponsored by the NSF under Cooperative Agreement 1852977. We thank Craig Feibel, Alan Robock, and Michael Mills for helpful discussion. BAB acknowledges support from NSF grant EAR 2015322. AS acknowledges funding from NERC grant NE/S000887/1 (VOL-CLIM).

Figures

Figure 1. Global-mean aerosol optical depth and surface temperature anomaly following 200 and 2000 Tg SO_2 Toba eruption scenarios. Ensemble means are shown as black lines. 2-sigma variability of ±0.4 °C in global mean monthly surface temperature in a 20 year control run is also shown.

Figure 2. Global-mean precipitation anomaly following 200 and 2000 Tg SO_2 Toba eruption scenarios. Gray shaded area shows natural variability, calculated as two standard deviations of the monthly global temperature anomaly in a 20-year control run relative to a monthly climatology.

Figure 3. Surface temperature anomalies on land in the second year following the Toba eruption. A. Annual mean global map, represented as the mean over 20 ensemble members for the 2000 Tg SO_2 Toba eruption scenario, with varying initial conditions. Hominin ranges from (60) and key proxy record and archaeological sites mentioned in the text are also shown. Hominin ranges are approximate, and incorporate significant uncertainty, for example due to continuing debate regarding the timing of dispersal of anatomically modern humans from Africa into Asia (61). B. Zonal means for 20 ensemble members for the 2000 Tg SO_2 scenario and 10 ensemble members for each 200 Tg SO_2 scenario. C. Annual mean map of Africa (inset region from A) D, Zonal means on land for the region shown in C. In A and C, cross-hatched areas indicate temperature anomalies that are not significant at the 90% level as determined with a Wilcoxon ranked sum test, compared with a monthly climatology from a 20-year control simulation.

Figure 4. Precipitation anomalies on land in the second year following the Toba eruption. A. Annual mean global map, averaging across 20 ensemble members for the 2000 Tg SO_2 eruption scenario as in Figure 3A. B. Zonal means on land with annual zonal-mean background precipitation on land shown as blue shaded areas. C. Enlargement of precipitation anomalies in Africa. D. Zonal means on land for the region shown in C. In A and C, cross-hatched areas indicate precipitation anomalies that are not significant at the 90% level as determined with a Wilcoxon ranked sum test, compared with a monthly climatology from a 20-year control simulation.

Figure 5. Likelihood of cooling and decreases in annual-mean precipitation reaching a specified threshold across 20 ensemble members with 2000 Tg SO_2 (panels A and B), 10 ensemble members with 200 Tg SO_2 at 35-40 km (panels C and D) and 10 ensemble members with 200 Tg SO_2 at 18-25 km (panels E and F). Panels A, C, and E show the fraction of runs predicting at least 4 °C cooling; panels B, D, and F show the fraction of runs predicting at least 40% decreases in precipitation on land for given regions.

References

1. Chesner CA & Luhr JF (2010) A Melt Inclusion Study of the Toba Tuffs, Sumatra, Indonesia. *J Volcanol Geotherm Res* 197(1): 259-278.

2. Costa A, Smith VC, Macedonio G & Matthews NE (2014) The Magnitude and Impact of the Youngest Toba Tuff Super-Eruption. *Frontiers in Earth Science* 2: 16.

3. Timmreck C*, et al* (2010) Aerosol Size Confines Climate Response to Volcanic Super-eruptions. *Geophys Res Lett* 37(24)

4. Lane CS, Chorn BT & Johnson TC (2013) Ash from the Toba Supereruption in Lake Malawi shows no Volcanic Winter in East Africa at 75 Ka. *Proc Natl Acad Sci U S A* 110(20): 8025-8029.

5. Roberts RG, Storey M & Haslam M (2013) Toba Supereruption: Age and Impact on East African Ecosystems. *Proc Natl Acad Sci U S A* 110(33): E3047.

6. Jackson LJ, Stone JR, Cohen AS & Yost CL (2015) High-Resolution Paleoecological Records from Lake Malawi show no Significant Cooling Associated with the Mount Toba Supereruption at Ca. 75 Ka. *Geology* 43(9): 823-826.

7. Yost CL, Jackson LJ, Stone JR & Cohen AS (2018) Subdecadal Phytolith and Charcoal Records from Lake Malawi, East Africa Imply Minimal Effects on Human Evolution from the~ 74 Ka Toba Supereruption. *J Hum Evol* 116: 75-94.

8. Petraglia M*, et al* (2007) Middle Paleolithic Assemblages from the Indian Subcontinent before and After the Toba Super-Eruption. *Science* 317(5834): 114-116.

9. Williams MA*, et al* (2009) Environmental Impact of the 73 Ka Toba Super-Eruption in South Asia. *Palaeogeogr , Palaeoclimatol , Palaeoecol* 284(3-4): 295-314.

10. Lane C*, et al* (2011) Cryptotephra from the 74 Ka BP Toba Super-Eruption in the Billa Surgam Caves, Southern India. *Quaternary Science Reviews* 30(15-16): 1819-1824.

11. Smith EI*, et al* (2018) Humans Thrived in South Africa through the Toba Eruption about 74,000 Years Ago. *Nature* 555(7697): 511-515.

12. Rampino MR & Self S (1992) Volcanic Winter and Accelerated Glaciation Following the Toba Super-Eruption. *Nature* 359(6390): 50-52.

13. Bekki S*, et al* (1996) The Role of Microphysical and Chemical Processes in Prolonging the Climate Forcing of the Toba Eruption. *Geophys Res Lett* 23(19): 2669-2672.

14. Robock A*, et al* (2009) Did the Toba Volcanic Eruption of~ 74 Ka BP Produce Widespread Glaciation?. *Journal of Geophysical Research: Atmospheres* 114(D10)

15. Ambrose SH (2000) Volcanic Winter in the Garden of Eden: The Toba Supereruption and the Late Pleistocene Human Population Crash. *Volcanic Hazards and Disasters in Human Antiquity* 345: 71.

16. Robock A (2000) Volcanic Eruptions and Climate. *Rev Geophys* 38(2): 191-219.

17. Ramanathan V, Crutzen PJ, Kiehl JT & Rosenfeld D (2001) Aerosols, Climate, and the Hydrological Cycle. *Science* 294(5549): 2119-2124.

18. Santer BD*, et al* (2015) Observed Multivariable Signals of Late 20th and Early 21st Century Volcanic Activity. *Geophys Res Lett* 42(2): 500-509.

19. Pinto JP, Turco RP & Toon OB (1989) Self‐limiting Physical and Chemical Effects in Volcanic Eruption Clouds. *Journal of Geophysical Research: Atmospheres (1984–2012)* 94(D8): 11165-11174.

20. Timmreck C*, et al* (2010) Aerosol Size Confines Climate Response to Volcanic Super‐eruptions. *Geophys Res Lett* 37(24)

21. Scaillet B, Clémente B, Evans BW & Pichavant M (1998) Redox Control of Sulfur Degassing in Silicic Magmas. *Journal of Geophysical Research: Solid Earth* 103(B10): 23937-23949.

22. Oppenheimer C (2002) Limited Global Change due to the Largest Known Quaternary Eruption, Toba≈ 74 Kyr BP?. *Quaternary Science Reviews* 21(14-15): 1593-1609.

23. English JM, Toon OB & Mills MJ (2013) Microphysical Simulations of Large Volcanic Eruptions: Pinatubo and Toba. *Journal of Geophysical Research: Atmospheres* 118(4): 1880-1895.

24. Timmreck C*, et al* (2012) Climate Response to the Toba Super-Eruption: Regional Changes. *Quaternary International* 258: 30-44.

25. McCormick MP, Thomason LW & Trepte CR (1995) Atmospheric Effects of the Mt Pinatubo Eruption. *Nature* 373(6513): 399-404.

26. Goddard L & Graham NE (1999) Importance of the Indian Ocean for Simulating Rainfall Anomalies Over Eastern and Southern Africa. *Journal of Geophysical Research: Atmospheres* 104(D16): 19099-19116.

27. Scholz CA*, et al* (2007) East African Megadroughts between 135 and 75 Thousand Years Ago and Bearing on Early-Modern Human Origins. *Proc Natl Acad Sci U S A* 104(42): 16416-16421.

28. Yang W, Seager R, Cane MA & Lyon B (2015) The Annual Cycle of East African Precipitation. *J Clim* 28(6): 2385-2404.

29. Held IM & Soden BJ (2006) Robust Responses of the Hydrological Cycle to Global Warming. *J Clim* 19(21): 5686-5699.

30. Iles CE, Hegerl GC, Schurer AP & Zhang X (2013) The Effect of Volcanic Eruptions on Global Precipitation. *Journal of Geophysical Research: Atmospheres* 118(16): 8770-8786.

31. Sigl M*, et al* (2015) Timing and Climate Forcing of Volcanic Eruptions for the Past 2,500 Years. *Nature* 523(7562): 543-549.

32. Pausata FS, Zanchettin D, Karamperidou C, Caballero R & Battisti DS (2020) ITCZ Shift and Extratropical Teleconnections Drive ENSO Response to Volcanic Eruptions. *Science Advances* 6(23): eaaz5006.

33. Khodri M*, et al* (2017) Tropical Explosive Volcanic Eruptions can Trigger El Niño by Cooling Tropical Africa. *Nature Communications* 8(1): 1-13.

34. McGregor S*, et al* (2020) The Effect of Strong Volcanic Eruptions on ENSO. *El Niño Southern Oscillation in a Changing Climate* : 267-287.

35. Aquila V, Oman LD, Stolarski RS, Colarco PR & Newman PA (2012) Dispersion of the Volcanic Sulfate Cloud from a Mount Pinatubo–like Eruption. *Journal of Geophysical Research: Atmospheres (1984–2012)* 117(D6)

36. Stevenson S, Fasullo JT, Otto-Bliesner BL, Tomas RA & Gao C (2017) Role of Eruption Season in Reconciling Model and Proxy Responses to Tropical Volcanism. *Proc Natl Acad Sci U S A* 114(8): 1822-1826.

37. Marshall L*, et al* (2019) Exploring how Eruption Source Parameters Affect Volcanic Radiative Forcing using Statistical Emulation. *Journal of Geophysical Research: Atmospheres* 124(2): 964-985.

38. Toohey M*, et al* (2019) Disproportionately Strong Climate Forcing from Extratropical Explosive Volcanic Eruptions. *Nature Geoscience* 12(2): 100-107.

39. Dai Z, Weisenstein D & Keith D (2018) Tailoring Meridional and Seasonal Radiative Forcing by Sulfate Aerosol Solar Geoengineering. *Geophys Res Lett* 45(2): 1030-1039.

40. Hurrell JW*, et al* (2013) The Community Earth System Model: A Framework for Collaborative Research. *Bull Am Meteorol Soc* 94(9): 1339-1360.

41. Marsh DR*, et al* (2013) Climate Change from 1850 to 2005 Simulated in CESM1 (WACCM). *J Clim* 26(19): 7372-7391.

42. Toon O, Turco R, Westphal D, Malone R & Liu M (1988) A Multidimensional Model for Aerosols: Description of Computational Analogs. *J Atmos Sci* 45(15): 2123-2144.

43. English J, Toon O, Mills M & Yu F (2011) Microphysical Simulations of New Particle Formation in the Upper Troposphere and Lower Stratosphere. *Atmos.Chem.Phys* 11(17): 9303-9322.

44. Bardeen CG, Garcia RR, Toon OB & Conley AJ (2017) On Transient Climate Change at the Cretaceous-Paleogene Boundary due to Atmospheric Soot Injections. *Proc Natl Acad Sci U S A* 114(36): E7415-E7424.

45. Gupta M & Marshall J (2018) The Climate Response to Multiple Volcanic Eruptions Mediated by Ocean Heat Uptake: Damping Processes and Accumulation Potential. *J Clim* 31(21): 8669-8687.

46. Svensson A*, et al* (2013) Direct Linking of Greenland and Antarctic Ice Cores at the Toba Eruption (74 Ka BP). *Climate of the Past* 9(2): 749-766.

47. Gleckler P*, et al* (2006) Krakatoa's Signature Persists in the Ocean. *Nature* 439(7077): 675-675.

48. Toohey M, Krüger K, Niemeier U & Timmreck C (2011) The Influence of Eruption Season on the Global Aerosol Evolution and Radiative Impact of Tropical Volcanic Eruptions. *Atmospheric Chemistry and Physics* 11(23): 12351-12367.

49. Haywood JM, Jones A, Bellouin N & Stephenson D (2013) Asymmetric Forcing from Stratospheric Aerosols Impacts Sahelian Rainfall. *Nature Climate Change* 3(7): 660-665.

50. Colose CM & LeGrande AN (2016) Hemispherically Asymmetric Volcanic Forcing of Tropical Hydroclimate during the Last Millennium. *Earth System Dynamics* 7(3): 681.

51. Sun W*, et al* (2019) How Northern High-Latitude Volcanic Eruptions in Different Seasons Affect ENSO. *J Clim* 32(11): 3245-3262.

52. Church JA, White NJ & Arblaster JM (2005) Significant Decadal-Scale Impact of Volcanic Eruptions on Sea Level and Ocean Heat Content. *Nature* 438(7064): 74-77.

53. Held IM & Soden BJ (2006) Robust Responses of the Hydrological Cycle to Global Warming. *J Clim* 19(21): 5686-5699.

54. Clarkson C*, et al* (2020) Human Occupation of Northern India Spans the Toba Super-Eruption~ 74,000 Years Ago. *Nature Communications* 11(1): 1-10.

55. Tabor CR, Bardeen CG, Ottoâ€↓Bliesner BL, Garcia RR & Toon OB (2020) Causes and Climatic Consequences of the Impact Winter at the Cretaceousâ€↓Paleogene Boundary. *Geophys Res Lett* 47(3): e60121.

56. Fasullo JT, Otto‐Bliesner BL & Stevenson S (2019) The Influence of Volcanic Aerosol Meridional Structure on Monsoon Responses Over the Last Millennium. *Geophys Res Lett* 46(21): 12350-12359.

57. Fasullo JT*, et al* (2017) The Amplifying Influence of Increased Ocean Stratification on a Future Year without a Summer. *Nature Communications* 8(1): 1-10.

58. Samset BH*, et al* (2018) Aerosol Absorption: Progress Towards Global and Regional Constraints. *Current Climate Change Reports* 4(2): 65-83.

59. Brown SC, Wigley TM, Otto-Bliesner BL, Rahbek C & Fordham DA (2020) Persistent Quaternary Climate Refugia are Hospices for Biodiversity in the Anthropocene. *Nature Climate Change* 10(3): 244-248.

60. Bae CJ, Douka K & Petraglia MD (2017) On the Origin of Modern Humans: Asian Perspectives. *Science* 358(6368): 10.1126/science.aai9067.

61. Mellars P, Gori KC, Carr M, Soares PA & Richards MB (2013) Genetic and Archaeological Perspectives on the Initial Modern Human Colonization of Southern Asia. *Proc Natl Acad Sci U S A* 110(26): 10699-10704.

62. Higham T*, et al* (2014) The Timing and Spatiotemporal Patterning of Neanderthal Disappearance. *Nature* 512(7514): 306-309.

63. Douka K*, et al* (2019) Age Estimates for Hominin Fossils and the Onset of the Upper Palaeolithic at Denisova Cave. *Nature* 565(7741): 640-644.

64. Vidal CM*, et al* (2016) The 1257 Samalas Eruption (Lombok, Indonesia): The Single Greatest Stratospheric Gas Release of the Common Era. *Scientific Reports* 6: 34868.

65. Manning JG*, et al* (2017) Volcanic Suppression of Nile Summer Flooding Triggers Revolt and Constrains Interstate Conflict in Ancient Egypt. *Nature Communications* 8(1): 1-9.

66. Zanchettin D*, et al* (2013) Background Conditions Influence the Decadal Climate Response to Strong Volcanic Eruptions. *Journal of Geophysical Research: Atmospheres* 118(10): 4090-4106.

67. Verschuren D, Olago DO, Rucina SM, Odhengo PO & ICDP DeepCHALLA Consortium (2013) DeepCHALLA: Two Glacial Cycles of Climate and Ecosystem Dynamics from Equatorial East Africa. *Scientific Drilling* 15: 72-76.

68. Garcia R, Marsh D, Kinnison D, Boville B & Sassi F (2007) Simulation of Secular Trends in the Middle Atmosphere, 1950â€“2003. *Journal of Geophysical Research: Atmospheres* 112(D9)

69. Sander S*, et al* (2006) . *Chemical Kinetics and Photochemical Data for use in Atmospheric Studies Evaluation Number 15*

70. Zielinski GA, Mayewski PA, Meeker LD, Whitlow S & Twickler MS (1996) A 110,000-Yr Record of Explosive Volcanism from the GISP2 (Greenland) Ice Core. *Quatern Res* 45(2): 109-118.

71. Crick L*, et al* (2021) New Insights into the~ 74 Ka Toba Eruption from Sulfur Isotopes of Polar Ice Cores. *Climate of the Past Discussions* : 1-28.

72. Chesner CA & Luhr JF (2010) A Melt Inclusion Study of the Toba Tuffs, Sumatra, Indonesia. *J Volcanol Geotherm Res* 197(1): 259-278.

73. Keppler H (1999) Experimental Evidence for the Source of Excess Sulfur in Explosive Volcanic Eruptions. *Science* 284(5420): 1652-1654.

74. Shinohara H (2008) Excess Degassing from Volcanoes and its Role on Eruptive and Intrusive Activity. *Rev Geophys* 46(4)

75. Smythe DJ & Brenan JM (2016) Magmatic Oxygen Fugacity Estimated using Zircon-Melt Partitioning of Cerium. *Earth Planet Sci Lett* 453: 260-266.

76. Chesner CA (1998) Petrogenesis of the Toba Tuffs, Sumatra, Indonesia. *J Petrol* 39(3): 397-438.

77. Costa A, Smith VC, Macedonio G & Matthews NE (2014) The Magnitude and Impact of the Youngest Toba Tuff Super-Eruption. *Frontiers in Earth Science* 2: 16.

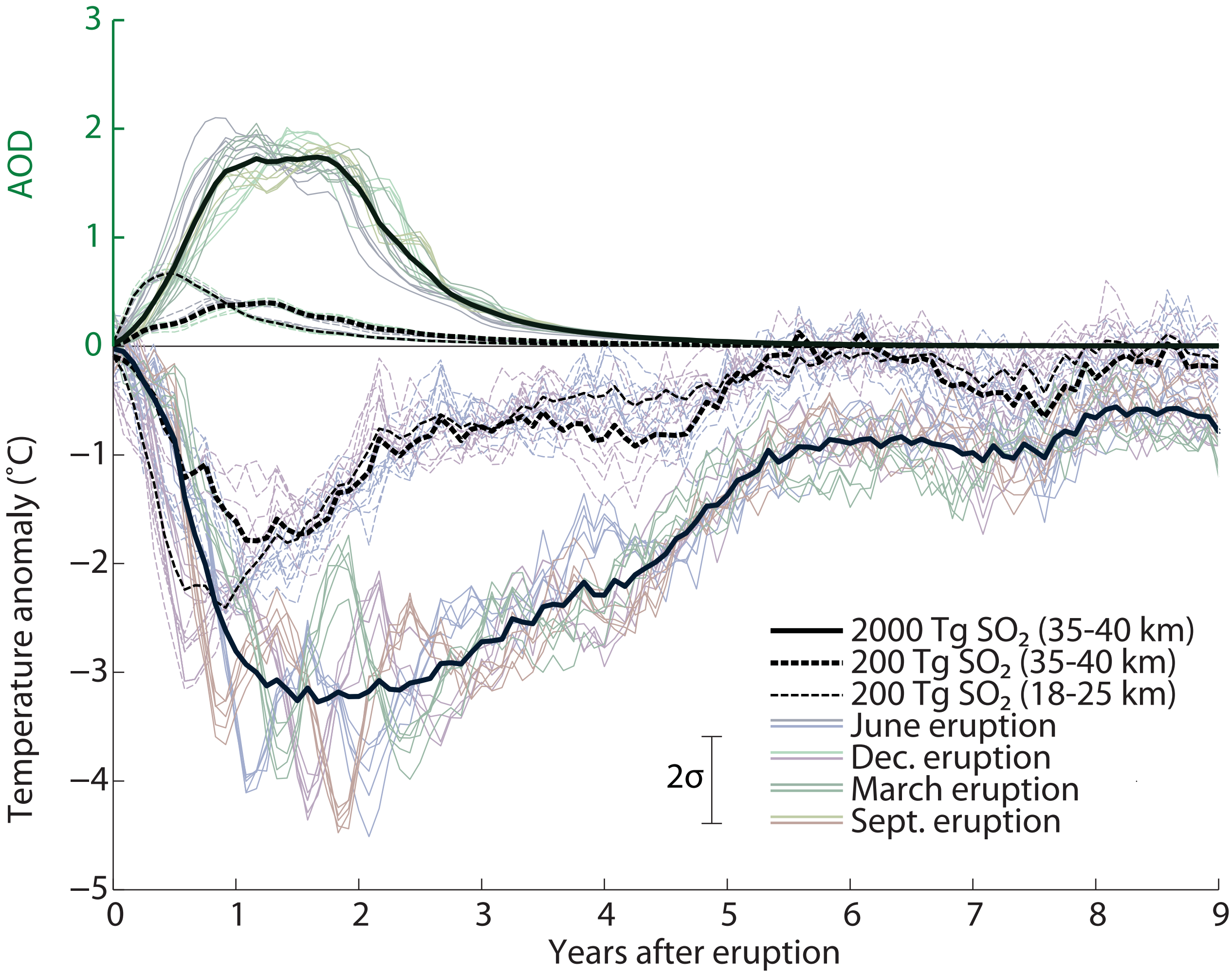

AOD
3
2
1
0
Temperature anomaly (°C)
−1
−2
−3
−4
−5
0
1
2
3
4
5
6
7
8
9
Years after eruption
2000 Tg SO2 (35-40 km)
200 Tg SO2 (35-40 km)
200 Tg SO2 (18-25 km)
June eruption
Dec. eruption
March eruption
Sept. eruption
2σ

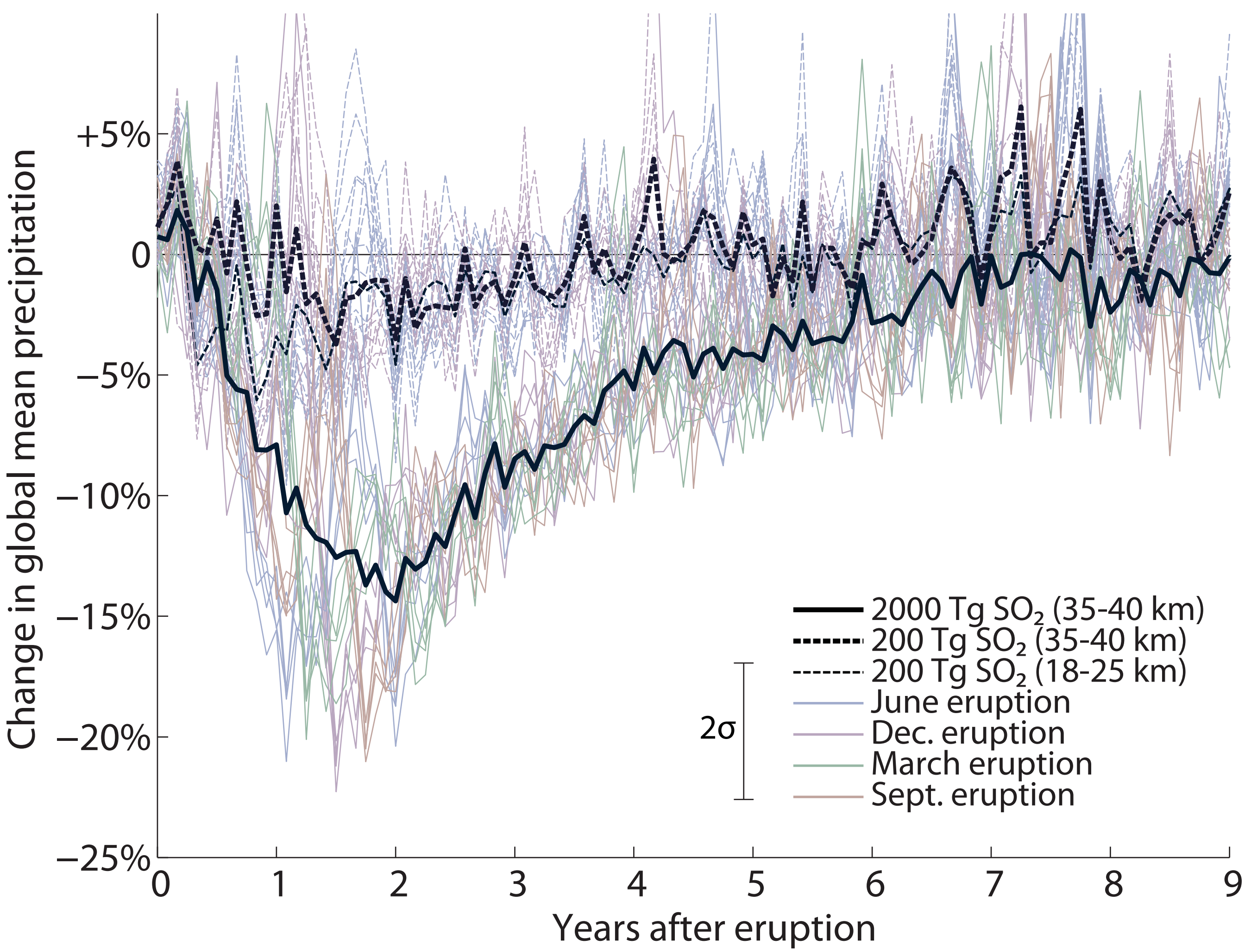
Change in global mean precipitation
+5%
0
−5%
−10%
−15%
−20%
−25%
0
1
2
3
4
5
6
7
8
9
Years after eruption
2000 Tg SO2 (35-40 km)
200 Tg SO2 (35-40 km)
200 Tg SO2 (18-25 km)
June eruption
Dec. eruption
March eruption
Sept. eruption
2σ

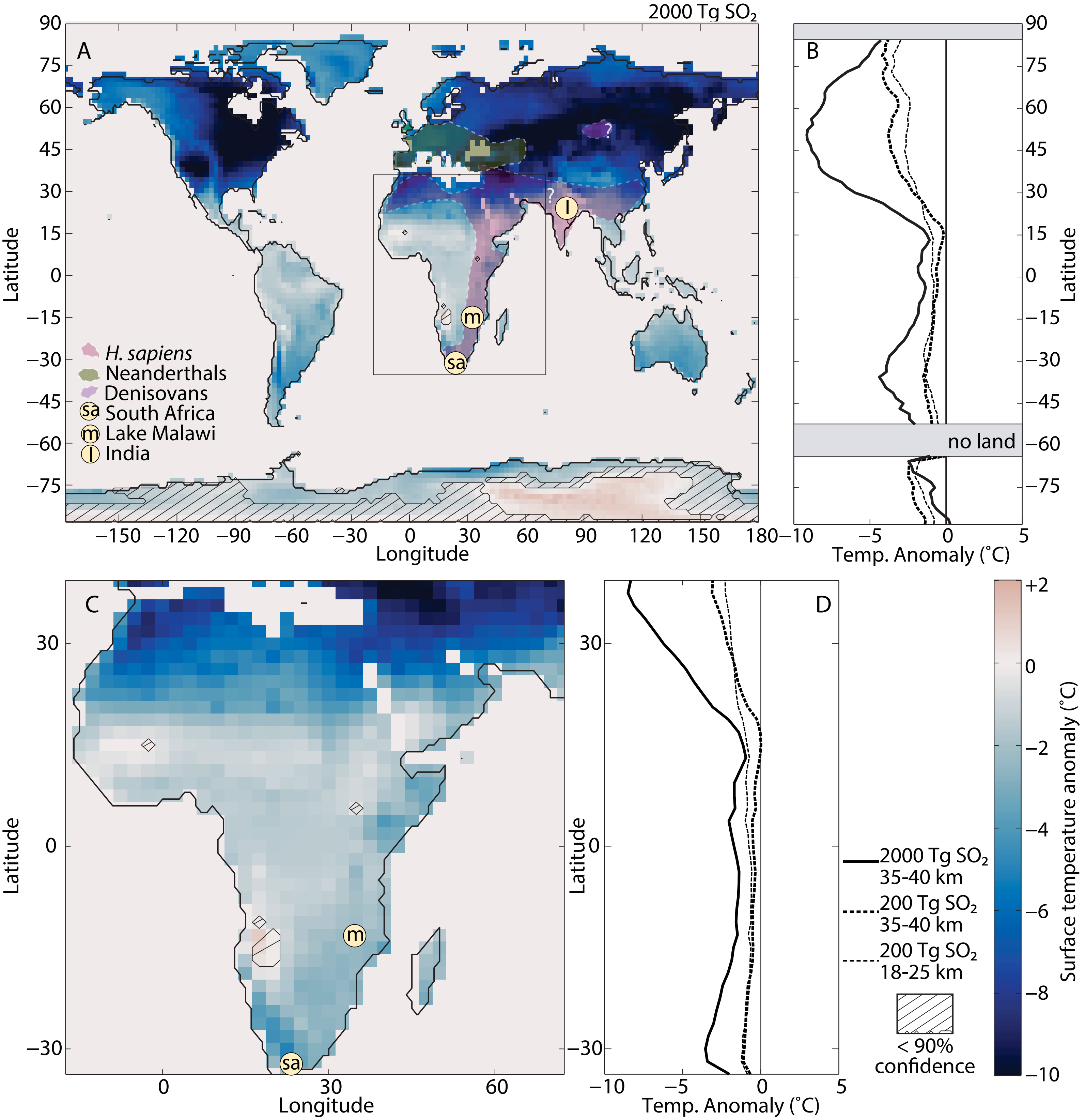

2000 Tg SO₂
A
B
C
D
H. sapiens
Neanderthals
Denisovans
sa South Africa
m Lake Malawi
I India
no land
Latitude
Longitude
Temp. Anomaly (˚C)
2000 Tg SO₂ 35-40 km
200 Tg SO₂ 35-40 km
200 Tg SO₂ 18-25 km
< 90% confidence
Surface temperature anomaly (˚C)

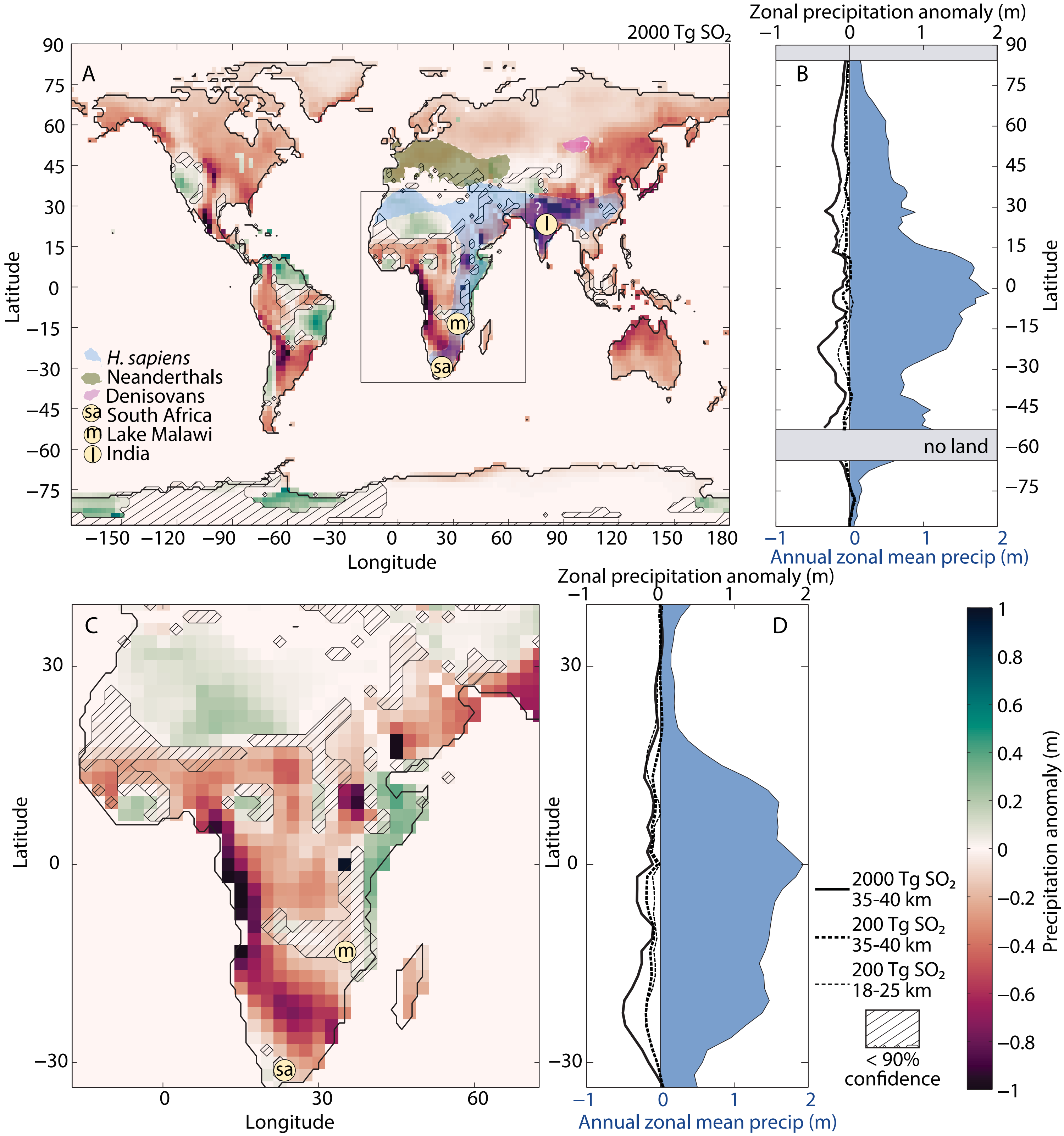

2000 Tg SO2
A
H. sapiens
Neanderthals
Denisovans
sa South Africa
m Lake Malawi
I India
Latitude
Longitude
B
Zonal precipitation anomaly (m)
Annual zonal mean precip (m)
no land
C
D
2000 Tg SO2 35-40 km
200 Tg SO2 35-40 km
200 Tg SO2 18-25 km
< 90% confidence
Precipitation anomaly (m)

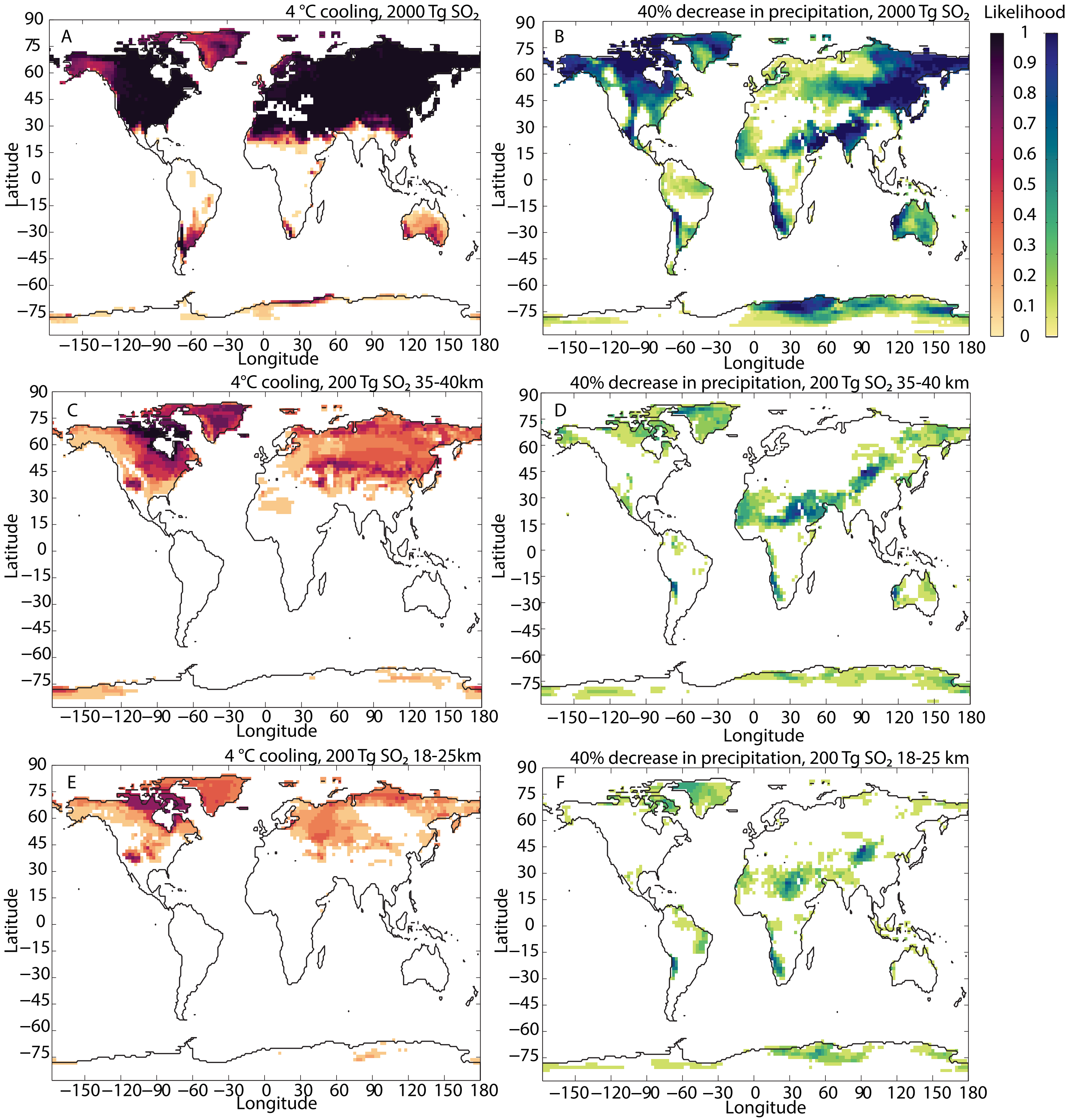

4 °C cooling, 2000 Tg SO_2
A
40% decrease in precipitation, 2000 Tg SO_2
B
Likelihood
1
0.9
0.8
0.7
0.6
0.5
0.4
0.3
0.2
0.1
0
4°C cooling, 200 Tg SO_2 35-40km
C
40% decrease in precipitation, 200 Tg SO_2 35-40 km
D
4 °C cooling, 200 Tg SO_2 18-25km
E
40% decrease in precipitation, 200 Tg SO_2 18-25 km
F
Latitude
Longitude
90
75
60
45
30
15
0
−15
−30
−45
−60
−75
−150
−120
−90
−60
−30
0
30
60
90
120
150
180